A Volcano Rekindled: The Renewed Eruption of Mount St. Helens, 2004–2006
Edited by David R. Sherrod, William E. Scott, and Peter H. Stauffer
U.S. Geological Survey Professional Paper 1750, 2008

Chapter 35

Trace Element and Pb Isotope Composition of Plagioclase from Dome Samples from the 2004–2005 Eruption of Mount St. Helens, Washington

By Adam J.R. Kent[1], Michael C. Rowe[2], Carl. R. Thornber[3], and John S. Pallister[3]

Abstract

We report the results of in-situ laser ablation ICP–MS analyses of anorthite content, trace-element (Li, Ti, Sr, Ba, La, Pr, Ce, Nd, Eu, Pb) concentrations, and Pb-isotope compositions in plagioclase from eight dome-dacite samples collected from the 2004–5 eruption of Mount St. Helens and, for comparison, from three dome samples from 1981–85. For 2004–5 samples, plagioclase phenocrysts range in composition from An_{30} to An_{80}, with the majority An_{42}–An_{65}. With the exception of Li, the range of trace-element abundances in plagioclase phenocrysts is largely constant in material erupted between October 2004 and April 2005 and is broadly consistent with the 1983–85 dome samples. Anomalously high Li contents in the early stage of the eruption are thought to reflect addition of Li to the upper part of the magma chamber immediately before eruption (within ~1 year) by transfer of an alkali-enriched, exsolved vapor from deep within the magma chamber. Other trace elements show significant correlations (at >99 percent confidence limits) with anorthite content in plagioclase phenocrysts—Ba, light rare-earth elements (LREE), and Pb show positive correlations, whereas Ti and Sr correlate negatively. Variations in plagioclase-melt partitioning as a function of anorthite content cannot explain trace-element variations—in particular predicting trends for Ti and Sr opposite to those observed. A simple model involving closed-system fractional crystallization of plagioclase + hypersthene + amphibole + oxides largely reproduces the observed trends. The model requires no gain or loss of plagioclase and is consistent with the lack of europium anomalies in bulk dacite samples. Analytical traverses within individual plagioclase phenocrysts support this model but also point to a diversity of melt compositions present within the magma storage zone in which plagioclase crystallized.

Plagioclase crystals from gabbronorite inclusions in three dacite samples have markedly different trace-element and Pb-isotope compositions from those of plagioclase phenocrysts, despite having a similar range of anorthite contents. Inclusions show some systematic differences from each other but typically have higher Ti, Ba, LREE, and Pb and lower Sr and have lower $^{208}Pb/^{206}Pb$ and $^{207}Pb/^{206}Pb$ ratios than coexisting plagioclase phenocrysts. The compositions of plagioclase from inclusions cannot be related to phenocryst compositions by any reasonable petrologic model. From this we suggest that they are unlikely to represent magmatic cumulates or restite inclusions but instead are samples of mafic Tertiary basement from beneath the volcano.

Introduction

Samples obtained from the 2004 eruption of Mount St. Helens provide an invaluable sample suite for application of petrological and geochemical techniques to examine the eruption of a silicic volcano. A wide range of approaches are detailed in this volume, and they provide valuable insight for monitoring of active and erupting volcanoes and for elucidating past eruptive histories on the basis of examination and analysis of eruptive materials.

This study reports measurements of trace-element abundances and Pb-isotope compositions in plagioclase from dome material erupted at Mount St. Helens from October 2004 to April 2005. The goals of the study are to apply the techniques of trace-element and isotope geochemistry to better

[1] Department of Geosciences, 104 Wilkinson Hall, Oregon State University, Corvallis, OR 97331

[2] Department of Geosciences, 104 Wilkinson Hall, Oregon State University, Corvallis, OR 97331; now at Department of Geoscience, 121 Trowbridge Hall, University of Iowa, Iowa City, IA 52242

[3] U.S. Geological Survey, 1300 SE Cardinal Court, Vancouver, WA 98683

understand origin and evolution of magma produced by the current eruption, as well as to demonstrate the utility of in-situ trace-element analyses by using laser-ablation inductively coupled plasma mass spectrometry (LA–ICP–MS) in petrological volcano-monitoring applications. The rapidity of this technique and relatively simple sample-processing requirements mean that, in the future, LA–ICP–MS could yield trace-element analyses of volcanic products on short time scales, providing an additional tool for monitoring anticipated and ongoing volcanic eruptions. Rowe and others (this volume, chap. 29) report on the application of these same techniques to document the chemistry of ash samples.

Samples and Methods

Samples

We have analyzed plagioclase in eight different dome samples collected between October 2004 and April 2005 and in a smaller number of plagioclase phenocrysts from three samples of earlier dome material erupted in September 1981 (SH100), May–June 1983 (SH141), and May 1985 (SH187) (table 1). Textural and compositional information from plagioclase is commonly used to elucidate the compositions of volcanic rocks (for example, Pearce and Kolisnik, 1990; Zellmer and others, 2003; Triebold and others, 2005; Browne and others, 2006; Streck and others, this volume, chap. 34). Our decision to concentrate on analysis of plagioclase reflects both the ubiquity of this mineral in all erupted products (typically ~80 percent of all crystalline phases and ~40 percent of the rock as a whole), as well as the observed textural diversity of plagioclase in dome samples. Plagioclase analyses, in conjunction with information on plagioclase-melt partition coefficients, also have the potential to act as a monitor of magma chemistry during crystallization (for example, Bindeman and others, 1998; Browne and others, 2006). In most of these samples, widespread groundmass crystallization makes direct analysis of liquid compositions difficult or impossible. Most dome samples contain little glass for analysis and, even where glass is found, it generally occurs only in restricted interstitial locations and has been clearly affected by late crystallization of groundmass phases. Our data supplement the extensive whole-rock geochemical datasets available for these samples (Pallister and others, this volume, chap. 30).

Table 1. Details of samples analyzed for this study.

[Estimates of eruption date are discussed in Pallister and others (this volume, chap. 30). Inclusions are from sample listed immediately above.]

Sample No.	Collection date	Estimated eruption date	Sample type	Number of analyses
2004–2005				
SH300-1A	10/20/04	<1986	Dacite dome	13
SH304-2A	11/4/04	10/18/04	Dacite dome	35[1]
SH304-2C	11/4/04	10/18/04	Dacite dome	17
Inclusion			Gabbronorite	15
SH305-1	1/3/05	11/20/04	Dacite dome	28
SH305-2	1/3/05	11/20/04	Dacite dome	10
Inclusion			Gabbronorite	10
SH306-1	1/14/05	12/15/04	Dacite dome	22
Inclusion			Gabbronorite	17
SH311-1	1/19/05	01/16/05	Dacite dome	17
SH315-1	4/19/05	04/1/05	Dacite dome	19
1981–85				
SH 100	9/8/81	September 1981	Dacite dome	6
SH 141	6/27/83	May–June 1983	Dacite dome lobe	8
SH 187	6/6/89	May 1985	Dacite dome	14

[1] Does not include 54 analyses from grain traverses.

Textural Classification

Studies of the Mount St. Helens dacite have shown some textural complexity in plagioclase and other crystalline phases (for example, Streck and others, this volume, chap. 34). However, in general, many of these features are observed at scales smaller than the 50–70-μm spatial resolution of the laser-ablation analysis used in this study. For this reason we have adopted a simplified textural classification for use with 2004–5 dome samples. This classification is also applicable to grains when polished sample mounts were viewed in reflected light. Most plagioclase occurs as euhedral or subhedral, equant to tabular phenocrysts less than 2 mm long. These display many of the features common in plagioclase phenocrysts from silicic magma, such as oscillatory zoning, spongy-textured zones, entrapment of melt inclusions, and some breakage of grains due to flow processes; but rounding of grains and resorbed zones are relatively uncommon. We refer herein to these crystals as plagioclase phenocrysts and interpret them as the result of crystallization of plagioclase directly from melt.

Plagioclase also is present in numerous crystal-rich inclusions in many recent Mount St. Helens lavas (Heliker, 1995). These generally are referred to as gabbroic inclusions, although many actually have gabbronoritic or noritic compositions and may be hornblende rich. Inclusions from the 2004–5 dacite appear similar to gabbroic and noritic inclusions from the 1980–86 dacite documented by Heliker (1995). In the 2004–5 dome material, inclusions occur in most recovered samples, although they are more abundant in some than others (for example, SH304-2C). We analyzed three hornblende-bearing gabbronorite inclusions from different samples (table 1) for this study. In these, plagioclase is relatively coarse (long axis as much as several millimeters) and subhedral to anhedral in form. Evidence of melt reaction and resorption is common along grain boundaries, suggesting that the inclusions are melting or reacting with the melt that transports them (Heliker, 1995). In thin sections, the inclusions can be seen to be in the process of actively disaggregating. Disaggregation results in a third textural type of plagioclase that we refer to as disaggregated inclu-

sions. Plagioclase crystals of this type occur isolated within the groundmass and are typically much larger than phenocrysts, as large as several millimeters, are subhedral or anhedral, and commonly show indications of significant resorption, disruption of zoning, and/or growth of new plagioclase on rims.

Analytical Methods

Samples were prepared for analysis by selecting small (~5–20 mm) pieces of dome lava from each sample and setting these in 25-mm-diameter epoxy mounts. In most cases, material was chosen because it was macroscopically representative of the larger sample, although in some cases pieces were selected to sample coarse-grained gabbroic inclusions. Once mounted in epoxy, samples were ground down several millimeters to expose the inside of the selected dacite piece by using coarse (240) grit paper before polishing with 300–600 grit paper and, finally, a 1-μm alumina powder and water slurry. Samples were then cleaned for ~5 minutes in distilled water in an ultrasonic bath, and mounts were photographed in reflected light and examined using backscattered electron imagery before analysis.

Trace-element measurements were made by LA–ICP–MS. All measurements were made in the W.M. Keck Collaboratory for Plasma Mass Spectrometry at Oregon State University using a DUV 193 nm ArF Excimer laser and a VG ExCell quadrupole ICP–MS. A general outline of the analytical techniques used for this instrument is given in Kent and others (2004a) and Kent and Ungerer (2006). Ablation was conducted under a He atmosphere, and He also was used to sweep resulting particulate into the ICP–MS at a flow rate of ~0.75 L/min.

During LA–ICP–MS, ~20–25 trace-element and internal-standard isotope masses were monitored (Kent and others, 2004a). Before each ablation, count rates were measured at each mass for 45 s to determine background count rates; these were then directly subtracted from the rates measured during ablation to account for the instrumental background. Following ablation, 45 s was allowed to elapse for signal washout before starting the next analysis. For all trace-element analyses the laser was held stationary relative to the sample so progressive ablation produced a circular crater. Ablation rates in silicate glasses and minerals are on the order of 0.1–0.2 μm per pulse, and a full ablation thus produced a crater 20–30 μm deep and resulted in ablation of ~100–400 ng of material. Two different analytical approaches were taken. First, in order to document trace-element variations between plagioclase phenocrysts and between these and plagioclase in gabbroic inclusions, a large number of analyses of plagioclase from multiple samples were made using 50–80-μm-diameter laser spots. During LA–ICP–MS analysis, detection limits depend largely on the rate at which material is removed, and these spot sizes provided sufficiently low detection limits to enable analysis of a range of trace elements (see below). Samples underwent ablation for 30–40 s with a laser pulse rate of 4 Hz. In addition, for sample SH304-2A a number of selected grains were analyzed along core-rim traverses using a smaller spot size (20 μm) and 7-Hz pulse rate. The smaller spot size allowed consistent detection of only the most abundant trace elements (Li, Ti, Sr, Ba, La, and Ce), but it provided higher spatial resolution to allow study of trace-element variations during progressive plagioclase crystallization. Plagioclase textures and major-element compositions of the same crystals analyzed in the trace-element traverse also were investigated using techniques similar to those detailed in Rowe and others (this volume, chap. 29) with backscattered electron imagery and wavelength-dispersive analysis using a Cameca SX-100 electron microprobe (EMPA).

Before calculation of trace-element abundances, background intensities for each mass were subtracted directly from those measured during ablation, and signals during ablation were only considered to be above background if they were greater than the background count rate plus three standard deviations (calculated from counting statistics). Estimates of minimum detection limits are: <1.5 μg/g for Ti and Li; <0.4 μg/g for Ba, and Rb; <0.1 μg/g for V, Sr, and Nd; and <0.05 μg/g for Y, Zr, Nb, Cs, La, Ce, Pr, Sm, Eu, Pb, Th, and U. In general, only Li, Ti, Sr, Ba, the light rare-earth elements (LREE: La, Ce, Pr, Nd), Eu, and Pb were consistently detectable, and we have restricted our study to these elements. Trace-element abundances were calculated with reference to NIST 612 glass with ^{29}Si as the internal standardizing isotope. Calculation of trace-element abundances required independent knowledge of the average SiO_2 content of each ablation volume, although in zoned plagioclase this may vary on spatial scales smaller than the laser spot size. For this reason, SiO_2 contents were determined directly from LA–ICP–MS analysis by exploiting the stoichiometric relation between anorthite content, CaO/SiO_2, and SiO_2 contents in plagioclase. Measured $^{43}Ca^+/^{29}Si^+$ ratios from plagioclase were converted to CaO/SiO_2 ratios by using the measurement of NIST 612 and application of equation 1:

$$\left(\frac{CaO}{SiO_2}\right)^{Calculated}_{Plagioclase} = \frac{\left(\frac{CaO}{SiO_2}\right)^{Known}_{NIST\_612}}{\left(\frac{^{43}Ca^+}{^{29}Si^+}\right)^{Measured}_{NIST\_612}} \times \left(\frac{^{43}Ca^+}{^{29}Si^+}\right)^{Measured}_{Plagioclase}, \quad (1)$$

where

$\left(\frac{CaO}{SiO_2}\right)^{Calculated}_{Plagioclase}$ is the calculated CaO/SiO_2 of the unknown plagioclase (with oxides in weight percent),

$\left(\frac{CaO}{SiO_2}\right)^{Known}_{NIST\_612}$ is the known CaO/SiO_2 of NIST 612 (we used 0.1594; Pearce and others 1997),

$\left(\frac{^{43}Ca^+}{^{29}Si^+}\right)^{Measured}_{NIST\_612}$ is the measured $^{43}Ca^+/^{29}Si^+$ ratio from NIST 612, and

$\left(\frac{^{43}Ca^+}{^{29}Si^+}\right)^{Measured}_{Plagioclase}$ is the measured $^{43}Ca^+/^{29}Si^+$ ratio in the unknown plagioclase.

We then calculated anorthite and SiO_2 contents of plagioclase from measured CaO/SiO_2 using equations 2 and 3:

$$SiO_2 = 36.02 \times \left(\frac{CaO}{SiO_2}\right)^{Calculated}_{Plagioclase} + 67.82\ , \quad (2)$$

and

$$An = 2.25 \times \left(\frac{CaO}{SiO_2}\right)^{Calculated}_{Plagioclase} + 0.019. \quad (3)$$

Equations 2 and 3 are based on empirical relations observed for Mount St. Helens plagioclase from electron microprobe analyses (M.C. Rowe and A.J.R. Kent, unpub. data, 2005) and are close to the those expected from stoichiometric considerations.

Results of measurement of USGS BCR-2G standard glass using the above protocol are shown in appendix 1. We also show CaO/SiO_2 ratios for these glasses calculated from equation 1, and these ratios are within uncertainty of the reported composition of this glass. In general, measured values agree closely with accepted values, and nearly all elements are within ± 5–10 percent of the accepted values.

One test of this analytical procedure is the comparison between anorthite contents measured by EMPA and LA–ICP–MS along the traverses in five plagioclase grains in sample SH304-2A (figs. 1, 2; appendix 2). Overall, there is good agreement between the two techniques, and where differences are apparent, they are most likely because the analyzed volume for LA–ICP–MS is significantly greater than the analyzed volume for EMPA. On the basis of reproducibility of CaO/SiO_2 ratios in BCR-2G, we believe that uncertainties in measured anorthite contents are ±5 percent mole fraction. Overall, we estimate uncertainties in trace-element measurements in plagioclase as ≤10 percent (at 2σ) for Sr, Ti, Ba, La, and Ce and ≤15–20 percent for Nd, Eu, Pb, and Li. Spot compositions of other Mount St. Helens plagioclase from 1981–85 and 2004–5 are given in appendix 3.

Lead isotope compositions of plagioclase phenocrysts, plagioclase in gabbroic inclusions, and groundmass were analyzed by laser-ablation multicollector ICP–MS (LA–MC–ICP–MS), using a NuPlasma multicollector ICP–MS at Oregon State University. Measurements were made using the same laser systems described above and using 80–100 μm laser spot size, pulse rate of 10–15 Hz, and a lateral translation rate of 5 μm/s. Individual measurements involved from three to five blocks, with each block consisting of two separate 10-s measurements, generally resulting in ablation along a track length of 300–500 μm. For measurement of groundmass composition, a relatively finely crystallized region was chosen and the laser spot simply was translated across the region while using the same ablation conditions. Although this produced some variation in signal intensity, the generally higher Pb content of this material resulted in data of relatively high quality. For most samples, signal intensity was too low (<<100 mV total Pb) to enable sufficiently precise measurement of the minor isotope ^{204}Pb, and thus we report only $^{208}Pb/^{206}Pb$ and $^{207}Pb/^{206}Pb$ ratios (appendix 1).

All ion beams were measured using Faraday collectors. Instrument mass bias was corrected by frequent measurement of NIST 612 and NIST 610 glass and by using the measured $^{208}Pb/^{206}Pb$ ratio to apply an exponential mass-bias correction to Pb-isotope ratios measured in unknown samples. Ratios of 2.1694 and 2.1651 for $^{208}Pb/^{206}Pb$ were measured by Baker and others (2004) in NIST 610 and NIST 612 and were used as the correct composition of this glass. Backgrounds were corrected by on-peak zero measurements for 30 s without the laser firing prior to analysis, with measured signals directly subtracted from signals measurement during ablation. Precision for individual analyses is strongly dependent on signal size and Pb abundance but is generally better than 0.2 percent for $^{208}Pb/^{206}Pb$ and $^{207}Pb/^{206}Pb$ ratios. Analysis of the BCR-2G glass standard gave results that are well within uncertainty of measurements made using solution techniques (Paul and others, 2005).

Results

Measured anorthite content for all plagioclase types ranges between An_{30} and An_{80}, with most between An_{42} and An_{68} (figs. 2, 3). Anorthite contents of plagioclase phenocrysts and those present within gabbroic inclusions show considerable overlap, although inclusions appear to show a somewhat more restricted range of compositions and may range to more anorthite-rich compositions (for example, grain 1 in fig. 2). Significant variations are evident in trace-element abundances in plagioclase, even where these are from the same sample, although the range of trace-element abundances from plagioclase phenocrysts from each sample is broadly similar, with the exception of Li. Lithium contents for dome samples erupted in October and November 2004 are consistently higher than those from subsequently erupted material (fig. 4; Kent and others, 2007; Rowe and others, this volume, chap. 29). Our results for plagioclase phenocrysts are indistinguishable from the composition of a smaller number of samples from the 1981–86 dome complex (fig. 3) and from sample SH300-1A, which is also considered to be a part of the 1980s dome complex pushed ahead of new erupting magma (Pallister and others, this volume, chap 30).

A correlation matrix for anorthite and trace-element abundances in plagioclase phenocrysts from all 2004–5 samples (a total of 138 analyses) shows significant correlations between anorthite content and the abundances of all trace elements other than Li in plagioclase phenocrysts (table 2; fig. 3): Sr and Ti are positively correlated and Ba, LREE, Eu, and Pb are negatively correlated with anorthite. For this relatively large number of analyses, correlation coefficients >0.17 and >0.23 are significant at the 95-percent and 99-percent confidence levels, respectively. Lithium shows no significant correlations with other elements, whereas Ba, LREE, and Pb are strongly positively correlated with each other. Strontium shows relatively poor correlations with Ti and La but signifi-

cant correlations with Ba, Eu, and Pb. Titanium shows significant negative correlations with Ba, LREE, Eu, and Pb.

There are clear differences in trace-element abundances between plagioclase phenocrysts and plagioclase from gabbroic inclusions. Plagioclase from inclusions typically has higher Ti, Ba, LREE, and Pb and lower Sr contents than phenocrysts with the same anorthite contents, and there also are some systematic differences between different inclusions (figs. 3, 4).

In general, analyses of groundmass and phenocrysts typically show similar Pb isotope composition, whereas plagioclase from gabbronorite inclusions have significantly different Pb-isotope compositions with lower $^{208}Pb/^{206}Pb$ and $^{207}Pb/^{206}Pb$ (fig. 5; appendix 1). In cases where groundmass was analyzed directly adjacent to disaggregating and reacting inclusions (for example, SH304-2C), groundmass compositions appear to lie along mixing lines between inclusions and groundmass from other samples.

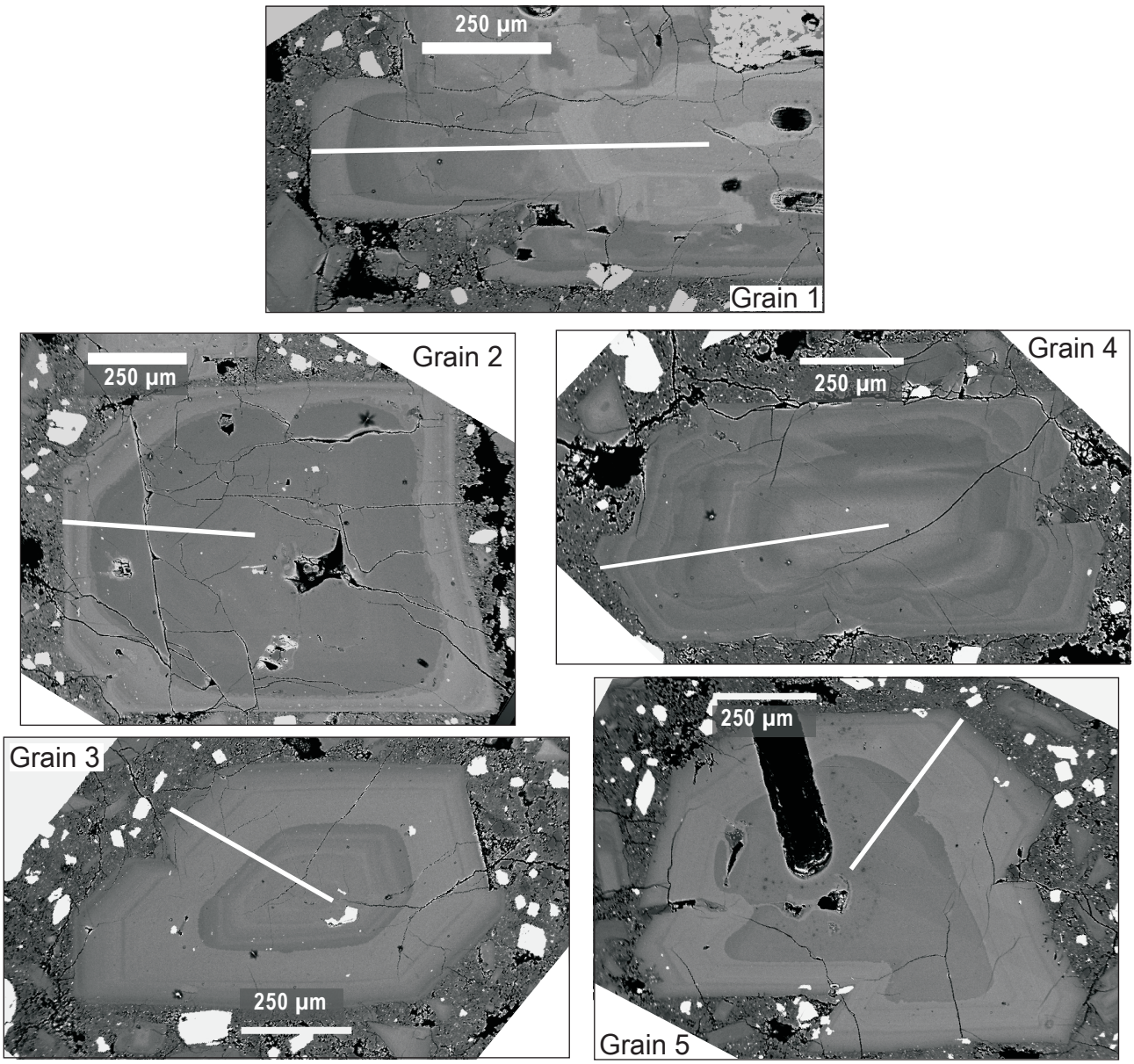

Figure 1. Backscattered electron images of five plagioclase grains from Mount St. Helens sample SH304-2A analyzed for major- and trace-element abundances along traverses. White line in each photograph shows location of analytical traverse.

Discussion

Compositional Variations Among Plagioclase Phenocrysts

Plagioclase phenocrysts from the 2004–5 dome samples show considerable variation in trace-element compositions, with abundances ranging by factors of ~3–5 over the range of anorthite contents recorded. Even at constant anorthite there is a factor of ~2–3 variation in trace-element abundances (fig. 3), which is far outside analytical errors. With the exception of Li, there is no systematic variation in the range of trace-element (fig. 4) or anorthite content in plagioclase phenocrysts over the course of the eruption, consistent with the lack of variation in whole-rock compositions (Pallister and others, this volume, chap. 30). In addition, there is no clear difference in trace-element composition of plagioclase

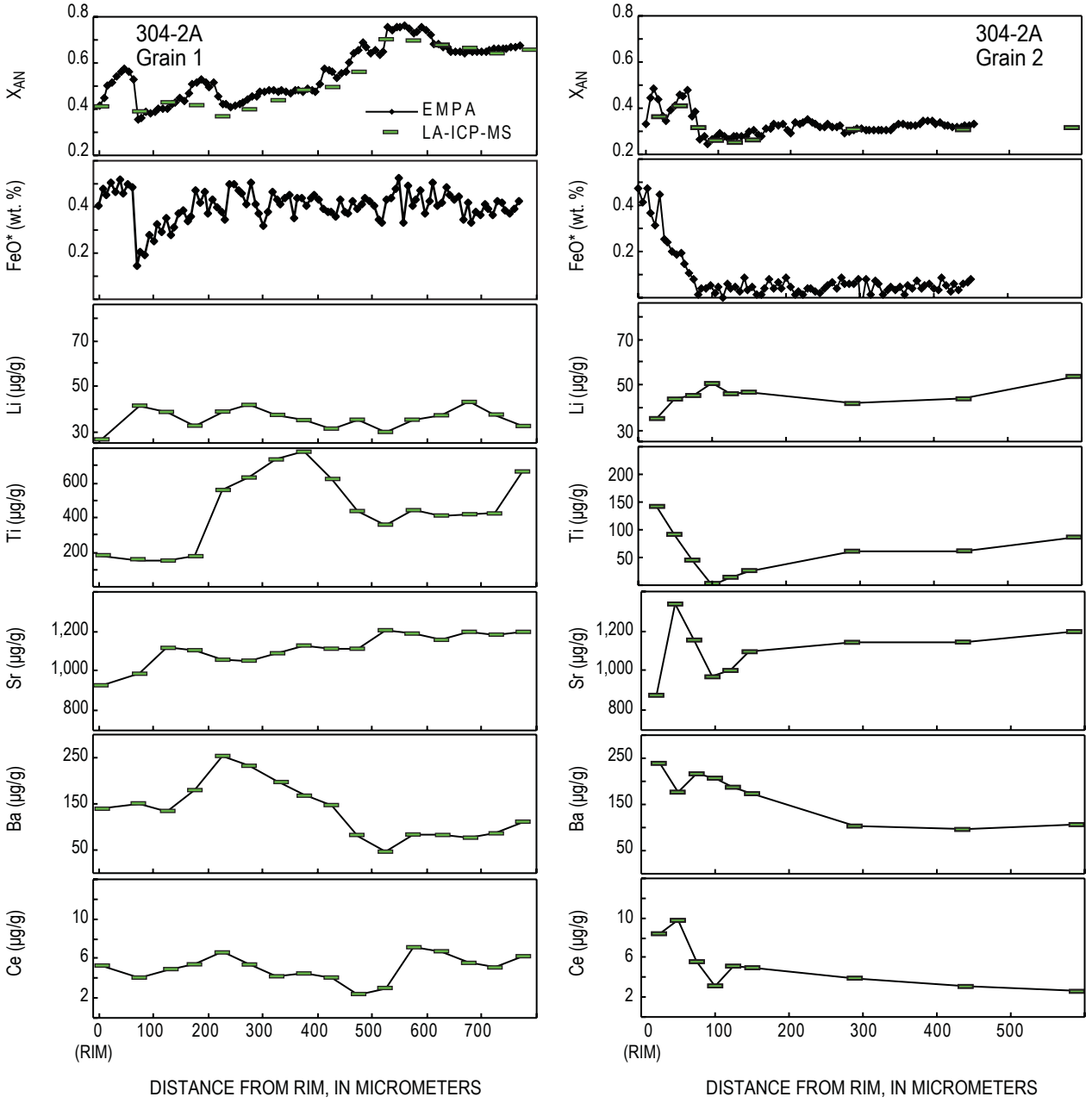

Figure 2. Mole-fraction anorthite (X_{AN}), FeO, Li, Ti, Sr, Ba, and Ce concentrations measured along traverses in five plagioclase grains from Mount St. Helens dacite sample SH304-2A (fig. 1). Symbol width for LA–ICP–MS data is the same size as the laser spot used. 0 is rim. All data except FeO are in appendix 2.

phenocrysts analyzed from 1981–85 dome samples and the 2004–5 samples (fig. 3), although there are suggestions that these samples originate from distinct magma batches (for example, Pallister and others, this volume, chap. 30; Blundy and others, this volume, chap. 33).

Abundances of trace elements other than Li show significant negative (Ba, LREE, Pb) or positive (Sr, Ti) correlations with anorthite content (table 2; fig. 3). One explanation for this is that the correlations simply reflect changes in plagioclase-melt partitioning with changing anorthite content (Blundy and Wood, 1994; Bindeman and others, 1998). However, although calculated plagioclase compositions (determined using the partitioning models in the preceding references and the bulk composition of 2004 dacite as a proxy for melt composition) are a reasonable match for the more incompatible elements (REE, Ba and Pb), the predicted trends for Sr and Ti are reverse to those evident in plagioclase phenocrysts (fig. 3).

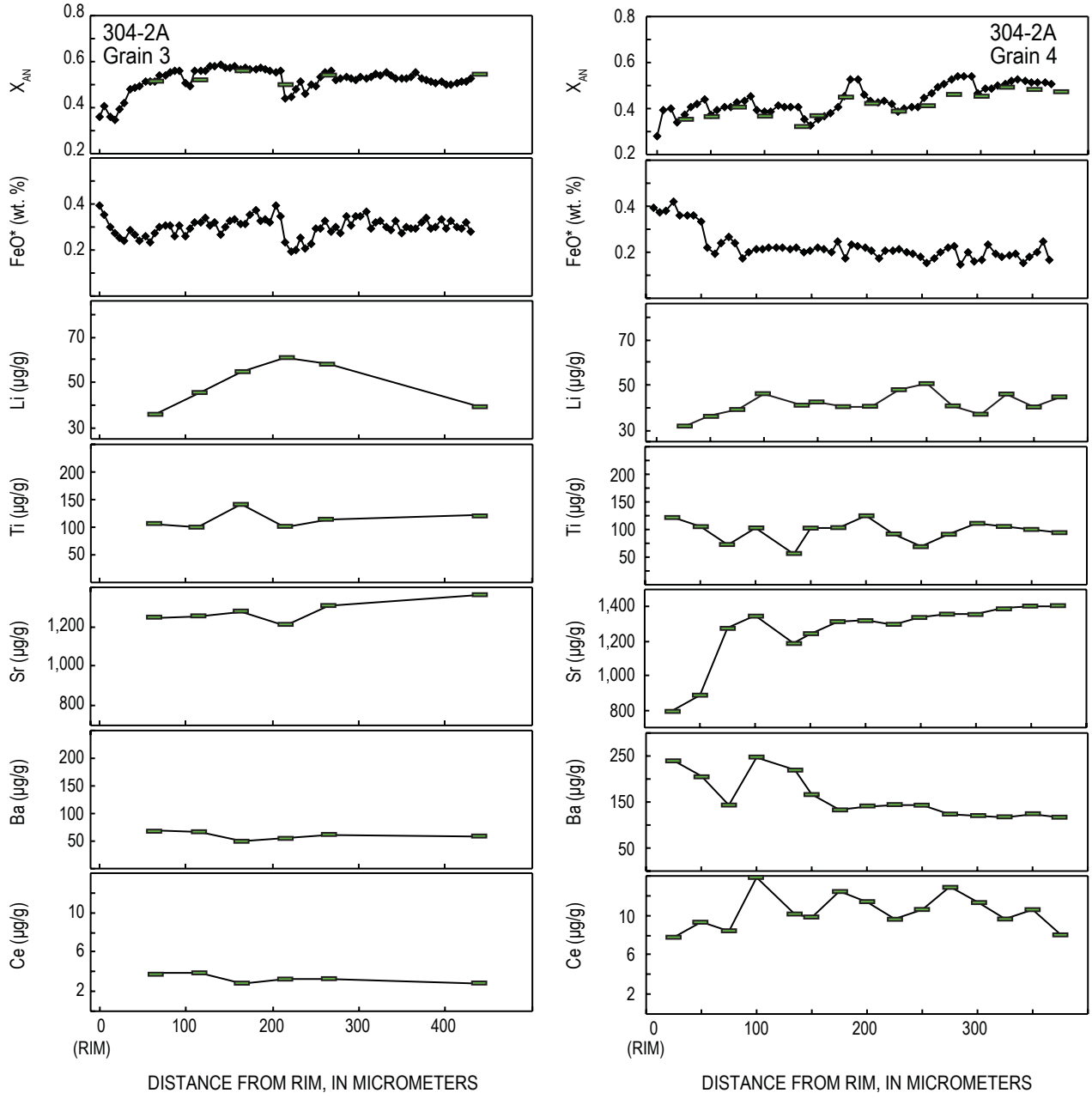

Figure 2.—Continued.

The simplest explanation for this observation is that decreases in Ti and Sr reflect removal of these elements from the melt during progressive closed-system crystallization of phenocryst phases. Because formation of crystals will sequester elements according to their partition coefficients, we do not need subsequent separation of crystals and liquid (as required to change the bulk composition) in order to change the composition of residual melt and subsequent crystals. The lack of europium anomalies in bulk dacite compositions (Pallister and others, this volume, chap. 30), together with simple calculations based on the Nd/Eu ratios of bulk dacite and feldspar, suggest that the 2004–5 dacite has lost <<5–10 percent plagioclase. The modal abundances of plagioclase and other phenocrysts observed in dacite samples thus probably approximate the overall proportions in which they have crystallized, a view broadly consistent with experimental investigations (Rutherford and Devine, this volume, chap. 31).

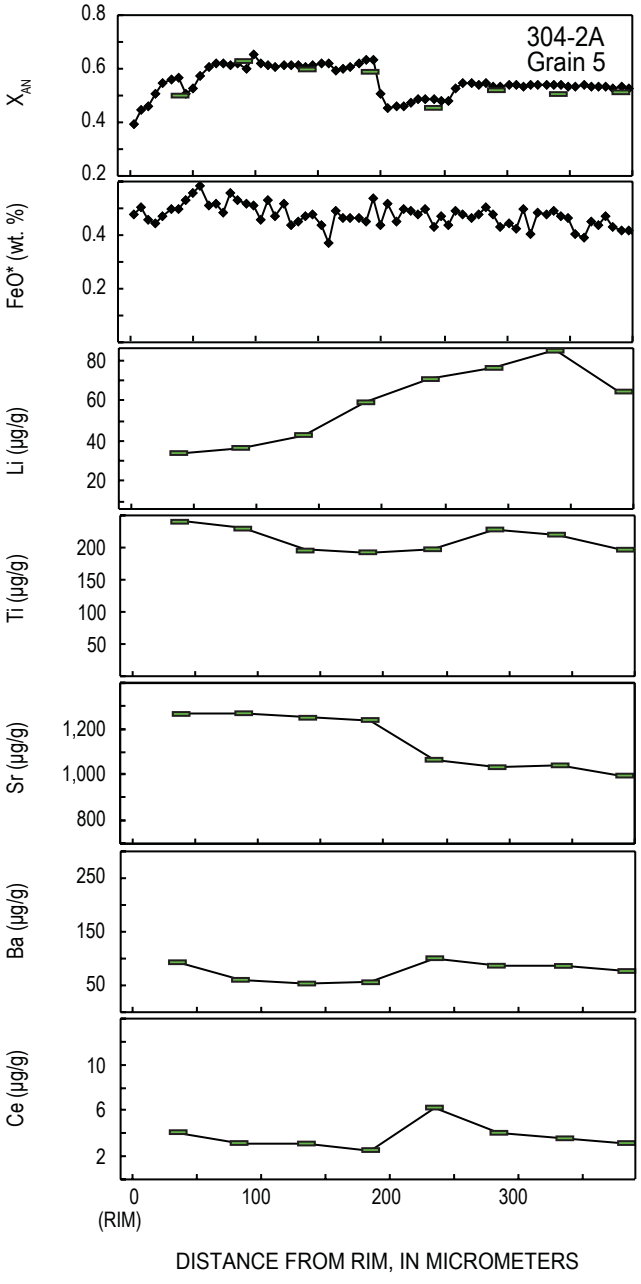

Figure 2.—Continued.

We have calculated changes in plagioclase composition using a simple model involving progressive crystallization of the observed phenocryst phases in the proportions in which they occur within the dacite from a melt with an initial composition that is the same as the bulk composition of dome dacite (fig. 6, table 3). Of the trace elements analyzed, Sr and Ti are the most compatible in the crystallizing assemblage of plagioclase, hypersthene, hornblende, and magnetite-ilmenite, with Sr entering plagioclase and Ti entering hornblende and ilmenite. We also note that our calculations are unlikely to fully explain all variations, given that we assume constant phase proportions and starting melt composition and that no accounting is made for differences in temperature, pressure, or reequilibration between plagioclase and melt (which may be significant for fast-diffusing elements such as Sr, according to Cherniak and Watson, 1994). However, the calculations do suggest that positive trends between anorthite contents and Sr and Ti, at least below ~An_{60}, could result from sequestration of these elements from melt during phenocryst growth and thus are linked to total crystallinity. Strontium/barium ratios in plagioclase also depart significantly from the trends expected from partitioning and are also largely replicated by our model. The negative correlations with anorthite shown by more incompatible elements (Pb, La, Ba) also are reproduced by our model, although these correlations do not differ significantly from those predicted by partitioning alone (fig. 3). Overall, we suggest that crystallization of the observed phenocryst phases, together with the control of anorthite content on crystal-liquid partitioning, exerts strong control over plagioclase trace-element abundances.

Control of mineral compositions by closed-system equilibrium crystallization is recognized in other crystal-rich, silicic magma systems (for example, Zellmer and others, 2003; Treibold and others, 2006), including Mount St Helens. Blundy and others (this volume, chap. 33) also suggest that closed-system crystallization controls glass inclusion compositions in 1980–86 Mount St. Helens lavas. Streck and others (this volume, chap. 34) argue that increases in crystallinity are the primary control on anorthite zoning in the outer ~80 µm of plagioclase phenocrysts in the 2004–5 eruption. Moreover this simple model does not necessarily conflict with more complex crystallization histories, as long as we consider trends shown by plagioclase to represent the range of histories experienced by individual plagioclase grains. Note that we do not visualize a simple "freezing" model in which a single homogenous melt crystallizes progressively until the current crystallinity is reached. Rather, as suggested by zoning and resorption features

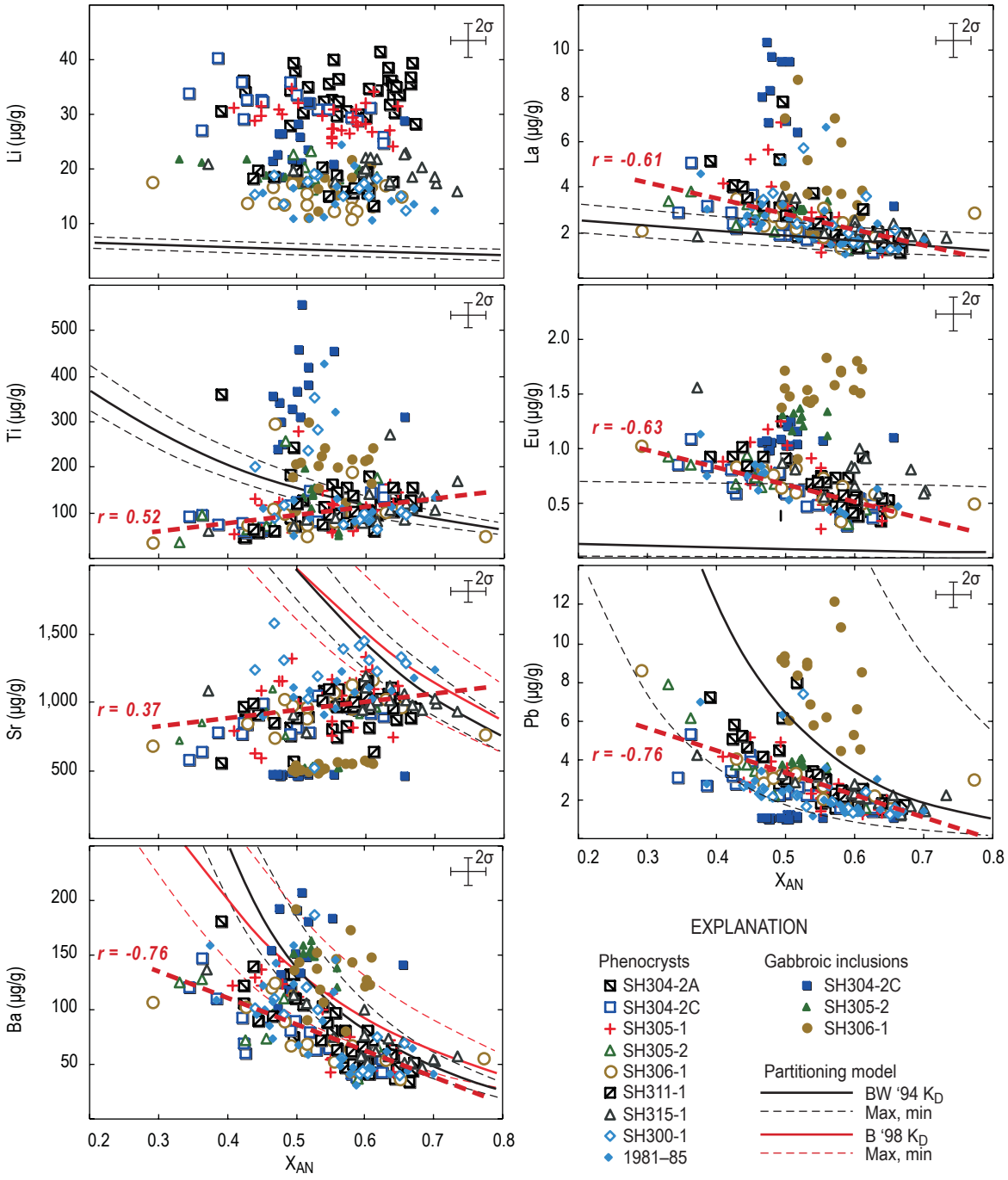

Figure 3. Trace-element abundances and anorthite content measured in plagioclase samples from Mount St. Helens dacite of 2004–5. Data shown for plagioclase present as phenocrysts and within gabbroic inclusions. Thick dashed red lines show linear least-squares fit to phenocryst data, with the value of the correlation coefficient *r* listed. No correlation shown for Li. Solid red and black lines show predicted elemental abundances in plagioclase calculated using plagioclase-melt partitioning models of Bindeman and others (1998; B '98) and, for Sr and Ba, Blundy and Wood (1994; BW '94), and the trace-element abundances measured in dacite sample SH304-2A (Pallister and others, this volume, chap. 30) as the estimated bulk melt composition (see text for explanation). All partition coefficients calculated at 850°C. Results for three dome samples (SH100, SH141, and SH187) from 1981–85 eruptions shown for comparison. Representative error bars (2σ) shown for each plot.

Table 2. Correlation matrix for anorthite and selected trace elements for plagioclase phenocrysts from 2004–2005 Mount St. Helens dome samples.

[Values shown are the calculated linear correlation coefficient *r*. For the number of analyses (n = 138) $|r| > 0.17$ is significant at 95-percent confidence, $|r| > 0.23$ is significant at 99-percent confidence.]

	Anorthite	Li	Ti	Sr	Ba	La	Eu	Pb
Anorthite	1	-0.04	0.52	0.37	-0.76	-0.61	-0.63	-0.76
Li	-0.04	1	0.14	-0.05	0.06	0.06	-0.04	-0.05
Ti	0.52	0.14	1	0.07	-0.23	-0.38	-0.31	-0.57
Sr	0.37	-0.05	0.07	1	-0.23	-0.11	-0.20	-0.24
Ba	-0.76	0.06	-0.23	-0.23	1	0.83	0.80	0.69
La	-0.61	0.06	-0.38	-0.11	0.83	1	0.74	0.66
Eu	-0.63	-0.04	-0.31	-0.20	0.80	0.74	1	0.68
Pb	-0.76	-0.05	-0.57	-0.24	0.69	0.66	0.68	1

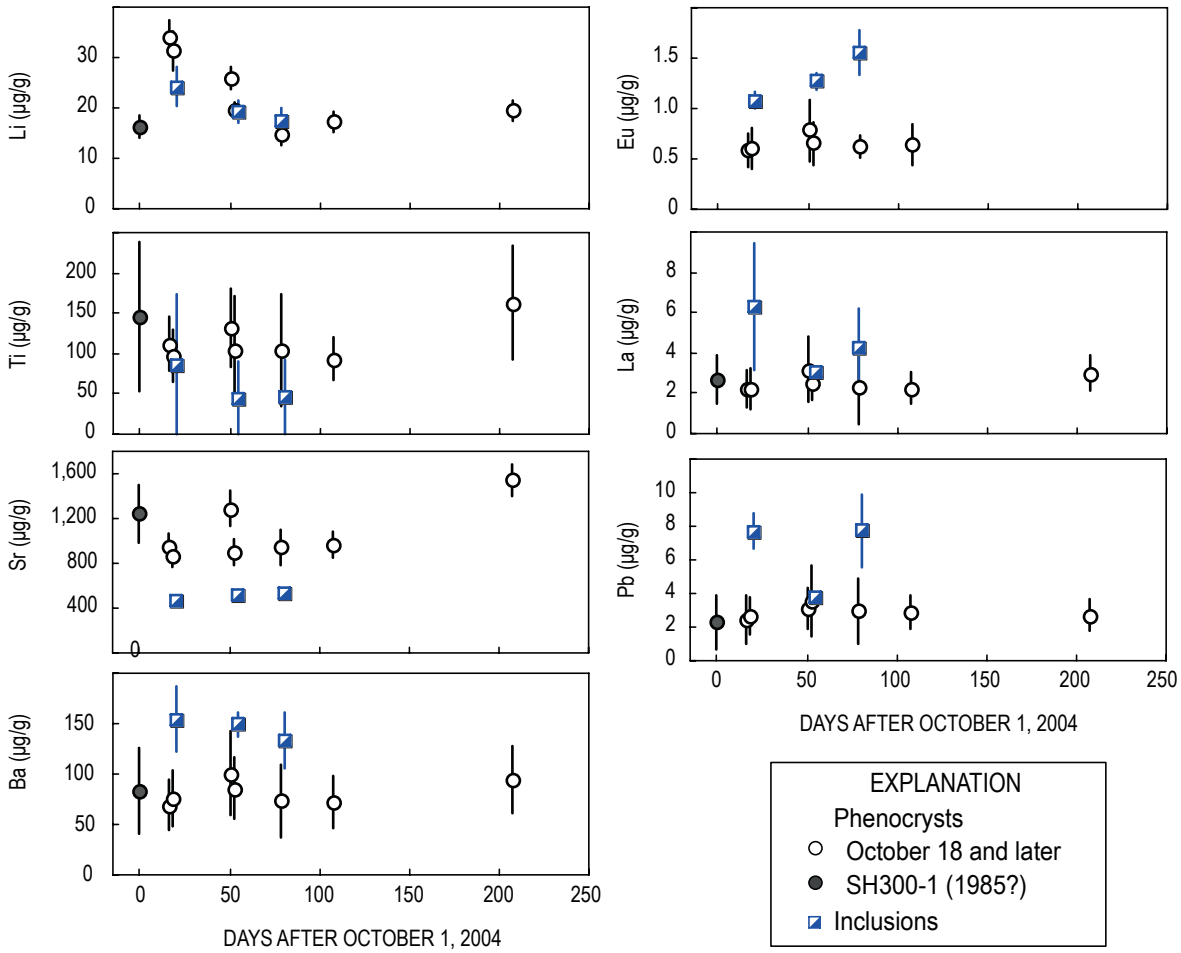

Figure 4. Average trace-element compositions of plagioclase phenocrysts and within gabbronorite inclusions from Mount St. Helens dacite collected between October 2004 and April 2005 as a function of estimated eruption date (Pallister and others, this volume, chap. 30). Symbols represent average composition ±1σ.

in plagioclase and other phenocrysts (see below; Rutherford and Devine, this volume, chap. 31; Streck and others, this volume, chap. 34), plagioclase phenocrysts experienced a range of pressure and temperature conditions and coexisted with a range of melt compositions within a convecting and self-mixing magma chamber (Couch and others, 2001; Rutherford and Devine, this volume, chap. 31). We discuss this further below.

Departures of Li and Eu in plagioclase from the predicted equilibrium partitioning values (fig. 3) are related to other factors. Variations in Li contents are discussed in further detail below and in Kent and others (2007). For Eu, the plagioclase-melt partition coefficients used in figure 3 are from the study of Bindeman and others (1998) and were measured from experiments conducted in the presence of atmospheric oxygen. In this case all Eu was present in the trivalent form, and thus Eu behaves consistently with the other moderately incompatible middle REE (K_D = ~0.1). In most volcanic systems, conditions are more reducing, significant amounts of more compatible divalent Eu are present, and Eu typically is more compatible in plagioclase than other REE (for example, Rollinson, 1993). If we use a general partition coefficient value of 2 for the plagioclase-melt partition coefficient (Rollinson, 1993), then we calculate more reasonable plagioclase Eu contents of 1–2 μg/g.

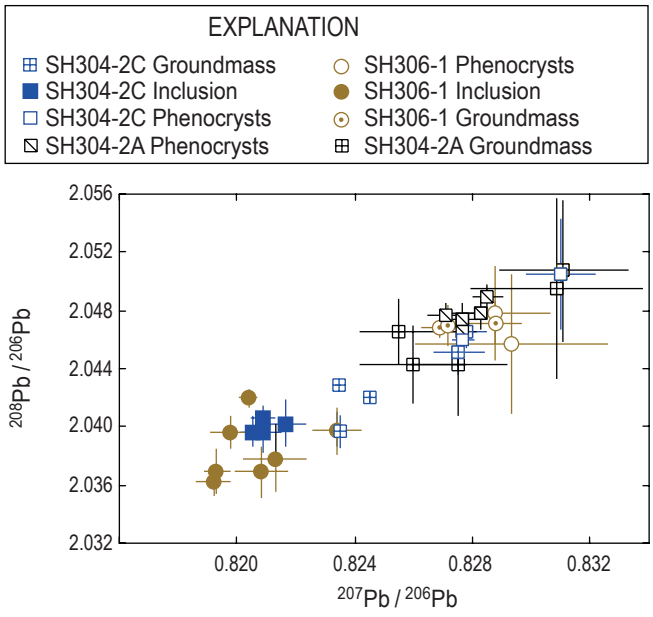

Figure 5. Measured $^{208}Pb/^{207}Pb$ and $^{207}Pb/^{206}Pb$ ratios of groundmass and plagioclase from phenocrysts and inclusions in three samples of 2004–5 Mount St. Helens dacite. Error bars represent 2σ error.

Compositional Variations Within Plagioclase Crystals

Anorthite, FeO, and trace elements were measured along traverses in selected plagioclase phenocrysts from SH304-2A to investigate changes in trace-element composition during progressive crystallization (figs. 1, 2). The grains chosen represent the general classes of phenocryst types recognized by Rutherford and Devine (this volume, chap. 31) and Streck and others (this volume, chap. 34).

The most common compositional feature of plagioclase phenocrysts is cyclic zoning, starting with an abrupt increase in An contents, sometimes also in conjunction with indications of mineral dissolution or resorption (for example, grain 5 in fig. 1), followed by more gradual decrease in An content until the start of the next cycle. Variations in the composition, number, and width of cycles are apparent in individual phenocrysts but, in general, the first plagioclase is $\geq An_{50}$, decreasing outward to ~$An_{40–20}$. This pattern recurs frequently; grain 4 shows multiple cycles, and grains 2, 3, and 5 show one or two cycles. Such cyclic compositional variation is common in plagioclase phenocrysts from the 2004–5 Mount St Helens dome, although there are subtle differences of opinion regarding their origin. Rutherford and others (this volume, chap. 31) suggest that these cycles represent plagioclase crystallizing during cycles of convection from deeper, hotter parts of the magma chamber to shallower and cooler conditions, whereas Streck and others (this volume, chap. 34) argue that anorthite cycles in the outer 80 μm of phenocrysts largely represent changes in crystallinity rather than changes in external conditions.

Although LA–ICP–MS analyses do not have sufficient spatial resolution to examine individual anorthite cycles in detail, trace-element abundances measured along traverses through individual grains can be examined in light of the variations evident between phenocrysts (figs. 3, 6). We have used the covariation between An contents and trace-element abundance as the basis for comparisons (fig. 7).

With some exceptions, trace-element variations within individual phenocrysts broadly follow the same general trends evident between plagioclase phenocrysts (fig. 2). Thus, within individual grains, Ti and Sr are positively correlated with anorthite, and An contents are broadly anticorrelated with Ba and La (for example, grains 2, 5). This relation also supports a model in which largely closed-system crystallization controls trace-element composition in coexisting liquid and subsequently formed plagioclase. However, in detail, individual crystals define separate subparallel trends (fig. 7). For example, Sr contents in grain 1 form a linear trend with positive slope that is offset to lower Sr contents at a given An than are similar trends in grains 2 and 4. In some cases, as with grain 4, analyses from a short segment of the traverse lie off the trend defined by the other analyses—specifically, the two outermost points measured on the rim have lower Sr and slightly higher Ti than the interior of the grain (figs. 2, 7). It is unlikely that changes in element partitioning related solely to anorthite or temperature

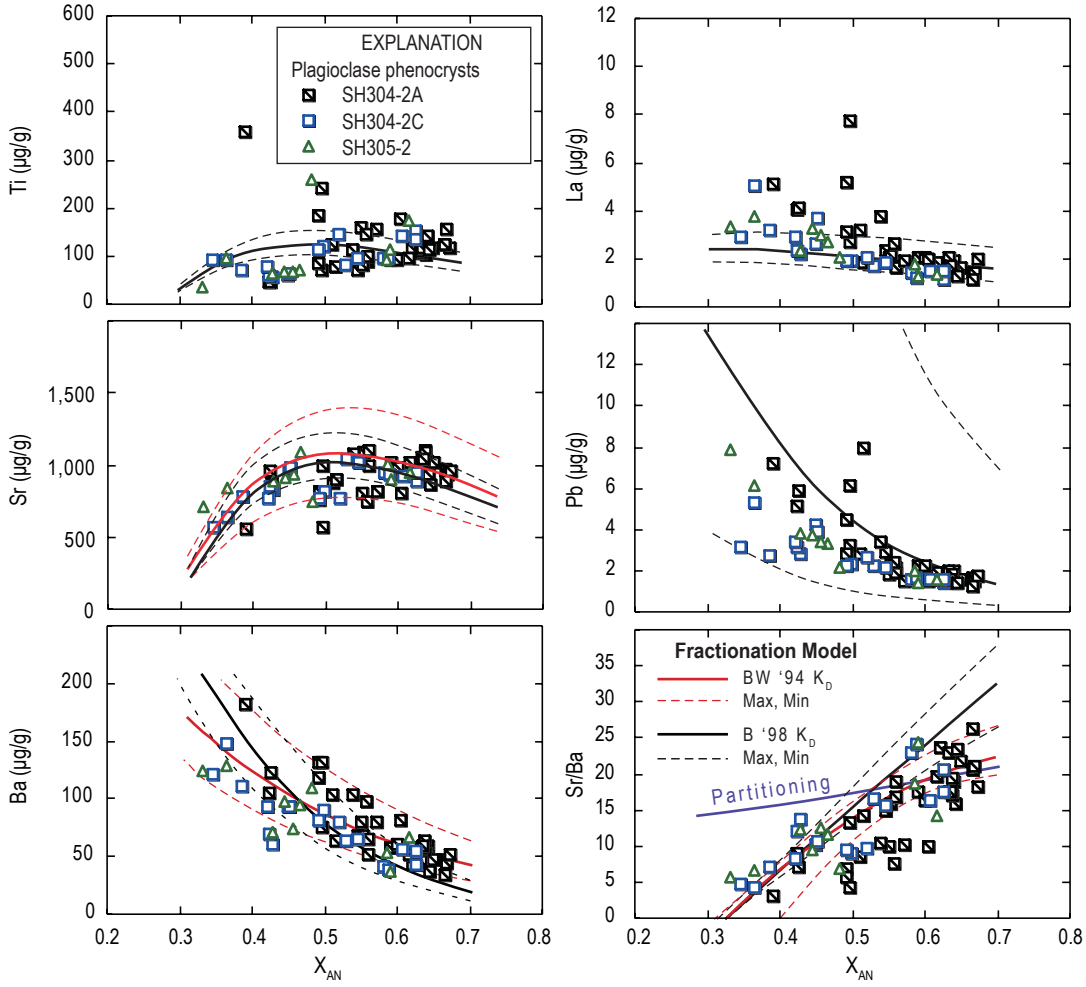

Figure 6. Comparison of selected trace elements and Sr/Ba ratios in plagioclase phenocrysts with trends predicted by a simple closed-system crystallization model. Only Mount St. Helens samples SH304-2A, SH304-2C, and SH305-2 are shown, for clarity, although these are broadly representative of other 2004–5 dome samples. Potential liquid lines of descent were calculated by incrementally removing plagioclase, hornblende, hypersthene, and oxides (magnetite and ilmenite in ratio 1: 5) from an initial melt of bulk composition similar to SH304-2. All phases were removed in the proportions in which they occur as phenocrysts within the dacite (table 3). Trace-element contents of ferromagnesian and oxide phases are given in table 3 and are based on preliminary analyses of these phases by electron microprobe (for Ti) and LA–ICP–MS. Note that the calculation is not particularly sensitive to variations in ferromagnesian and oxide compositions owing to the low modal proportions of these phases and their generally low trace-element contents. The exception is Ti, which is relatively abundant in hornblende (TiO_2 ~2–3 wt. percent) and in ilmenite (TiO_2 ~50 wt. percent). For every 2-percent increment of crystallization, trace-element abundances of equilibrium plagioclase were calculated using the partitioning models of Bindeman and others (1998; black lines) and, for Sr and Ba, Blundy and Wood (1994; red lines). All partition coefficients were calculated at 850°C, consistent with current estimates of magmatic temperatures for 2004–5 (Pallister and others, this volume, chap. 30), although the model is not significantly different at higher temperatures. Uncertainties in partition coefficients shown by dashed lines associated with predicted trends from each partitioning model. Because the anorthite content of crystallizing plagioclase is dictated by several factors (for example, volatile contents, pressure, temperature, and composition), we chose to crystallize the first plagioclase at An_{70} composition and to have the anorthite content decrease linearly and progressively until the final plagioclase has a composition of An_{35} after crystallization of 54 weight percent, the total amount of phenocrysts observed in sample SH304-2A on a void-free basis (Pallister and others, this volume, chap. 30). The change in Sr/Ba ratio predicted by partitioning (using the partition coefficients of Bindeman and others, 1998) is shown by the purple line.

Table 3. Mineral and magma compositions used for crystal-fractionation model shown in figure 6.

[Column labeled Crystal proportion is that observed in dacite sample SH304-2A (Pallister and others this volume, chap. 30), calculated on a groundmass-free basis and not including plagioclase microphenocrysts in groundmass. For oxide minerals, Ti content represents crystallization of magnetite:ilmenite in ratio of ~5:1 (Pallister and others, this volume, chap. 30). Not shown are plagioclase trace-element contents, which were calculated separately for each increment of plagioclase crytallized from the coexisting melt composition, using the partitioning relations of Bindeman and others, (1998). Starting magma composition based on whole-rock analyses of 2004–2005 dome material (Pallister and others, this volume, chap. 30).]

Phase	Crystal proportion	Ti	Sr	Ba	La	Ce	Eu	Pb
Hypersthene	0.10	900	10	1	1	2	0.1	0.1
Hornblende	0.06	30,000	50	70	1	2	0.3	1.7
Oxide	0.02	100,000	0	0	0	0	0	0
Plagioclase	0.82							
Starting magma		4,000	400	336	15	30	1.3	9.8

variations are sufficient to produce the variations found between crystals. We suggest that plagioclase compositions also reflect variations in the composition of coexisting melt from which plagioclase crystallized. Although compositional variations could be inherited partly from the mid or lower crustal source of the dacitic magmas, the near-constant composition of 2004–5 bulk dacite samples argues against large source-derived variation (Pallister and others, this volume, chap. 30). We suggest instead that localized variations in *P* and *T*, crystallinity, and proportions of crystallizing phases within the magma storage zone result in localized variations in melt composition. Crystals reflect the composition of localized melt(s) from which they grow, and thus individual crystals record variable composition trends. Occasional juxtaposition of crystals with new melt compositions, possibly related to convective stirring, also results in crystals with compositions that depart from well-defined trends on variation diagrams, as seen in Sr and Ti in grain 4. We note that melt inclusions from 1980–86 and 2004–5 samples also show large differences in Ba and REE abundances at similar SiO_2, consistent with diverse melt compositions during mineral growth (Blundy and others, this volume, chap. 33).

Grain 1 is slightly different from the other grains analyzed. It is part of a large, complex plagioclase glomerocryst and has a complex anorthite-rich core (as high as An_{75}) with an adjacent low-anorthite central part and then two cycles of $An_{55–60}$ to $An_{38–40}$ (fig. 2). This grain has Ti contents as high as ~600 μg/g in its inner region (from ~200 to 700 μm from the rim), which are considerably higher than the Ti contents of other plagioclase phenocrysts (fig. 3). High Ti suggests that the core of this crystal might have been derived from a disaggregated gabbroic inclusion, although other trace elements do not have inclusion-like compositions. In particular, Sr abundances in the core of this grain are ~1,000–1,200 μg/g, unlike the ~500 μg/g contents seen in plagioclase within gabbroic inclusions (fig. 3). Although the origin of this grain is uncertain, the high Sr might reflect further heterogeneity among inclusions (fig. 3), or it could be due to reequilibration of Sr in plagioclase with melt after disaggregation, with more slowly diffusing Ti not yet reequilibrated (compare with Zellmer and others, 2003). The latter explanation requires a residence time of several thousand years to reequilibrate over distances of hundreds of microns.

Lithium Variations in Plagioclase Phenocrysts

Variations in the Li contents in 2004–5 dome and ash samples are of particular interest and have been discussed in detail by Kent and others (2007) and Rowe and others (this volume, chap. 29). As shown in figure 4, Li contents in plagioclase phenocrysts erupted at the onset of dome extrusion are anomalously high (samples SH304-2A, SH304-2C). These concentrations are higher, by about a factor of two, than those seen in subsequently erupted material and in sample SH300-1 (interpreted to be a remnant of 1980s dome material), and this difference is significant to >99 percent confidence. The increase in Li in October–November 2004 samples mirrors that reported by Berlo and others (2004) in plagioclase from the 1980 eruption of Mount St. Helens, in which high Li contents in plagioclase phenocrysts erupted prior to May 18 and cryptodome material erupted May 18 are thought to reflect vapor-phase transport of alkali metals during degassing from deep within the magma storage zone before eruption (Berlo and others 2004; Blundy and others, this volume, chap. 33). Kent and others (2007) suggest a similar model to explain the 2004–5 material. Although Li contents in the bulk magma from October and November 2004 are not elevated (Pallister and others, this volume, chap. 30), this is probably as a result of vapor loss during late shallow (< ~10 MPa) degassing (Kent and others, 2007). Lithium diffusion in plagioclase is slower than in melt, and thus plagioclase preserves the high Li signature, provided decompression and cooling are sufficiently rapid. This model is supported by the measurement of Li concentrations as high as 207 μg/g in melt inclusions from SH304-2A (Kent and others, 2007) and in Li-loss profiles evident in the outer 100–300 μm of plagioclase transects (fig. 2). High Li signatures also are evident in ~20 percent of pla-

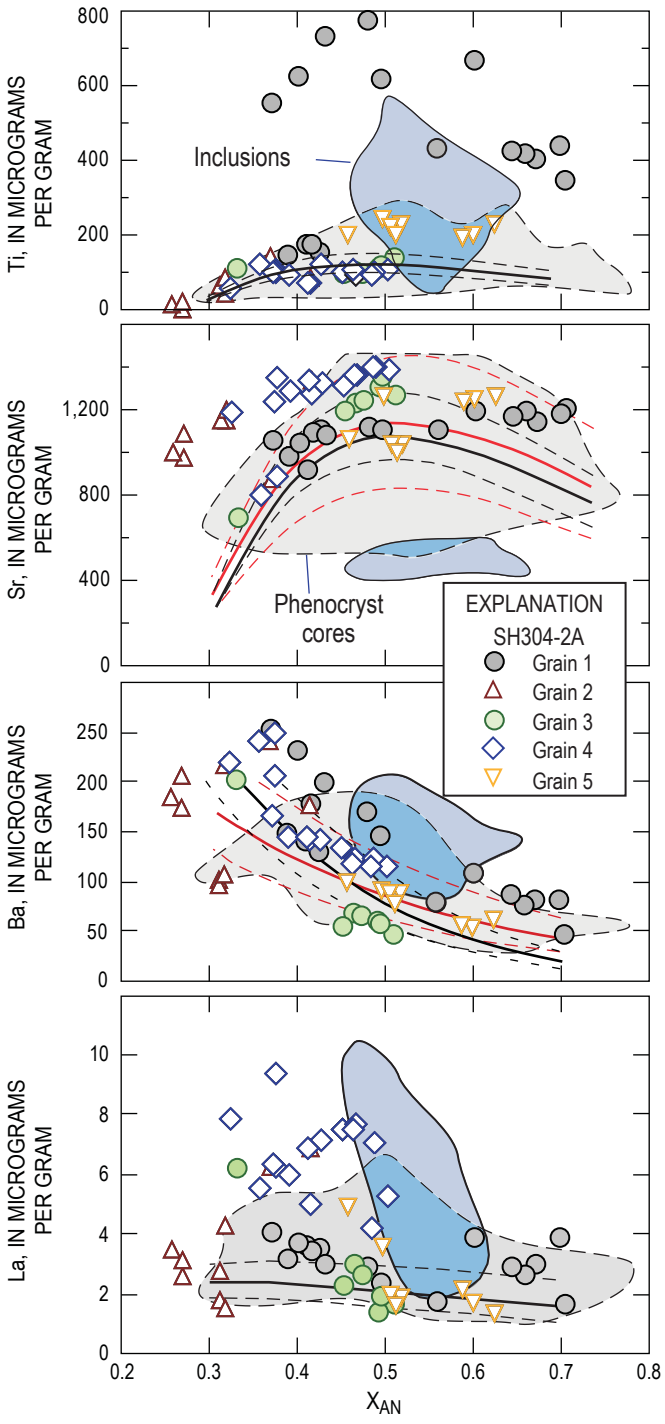

Figure 7. Ti, Sr, Ba, and La versus mole fraction anorthite (X_{AN}) content measured along plagioclase traverses (see figs. 1, 2). Fractionation models from figure 6 are shown as black and red lines (see fig. 6 caption for details). Fields show the range of compositions measured in plagioclase phenocrysts (gray field, dashed line) and gabbroic inclusions (blue field, solid line), from figure 3.

gioclase in ash from explosive eruptions on October 1–5, 2004, as noted by Rowe and others (this volume, chap. 29), who suggest that these explosions were phreatomagmatic in origin. Finally, diffusion modeling based on differences between Li contents in plagioclase phenocrysts and gabbroic inclusions in SH304-2C (fig. 4) suggests that Li enrichment occurred relatively recently—probably within a year of eruption (Kent and others, 2007). One plausible scenario is that the accumulation and phase separation of vapor in the apical part of the shallow Mount St. Helens magma chamber (~5 km) resulted in increased fluid pressure before eruption. Rupturing of wallrocks in late September 2004, perhaps induced by increases in fluid pressure, resulted in loss of the low-density vapor and reequilibration between a high-density, Li-bearing vapor phase and magma. After upward movement of magma commenced in late September or early October, Li-enriched apical magma contributed to initial phreatomagmatic explosions in early October (Rowe and others, this volume; chap. 29) and was the first material erupted once extrusion commenced. Comparison with eruption rates suggests that Li-enriched magma represents ~15–20 percent of the volume of the total material erupted.

Composition and Origin of Gabbronorite Inclusions

Mafic plutonic inclusions are a common feature of Mount St. Helens lavas from the last ~3,000 years and are relatively common in 2004–5 dome samples (Pallister and others, this volume, chap. 30). The potential sources for mafic inclusions include crystalline cumulates and crystal-rich wallrock zones (Heliker, 1995; Cooper and Donnelly, this volume, chap. 36) and fragments of basement rock removed from conduit walls and transported within the magmatic system. One key issue is whether these inclusions represent parts of the same magmatic system responsible for generation and transport of Mount St. Helens magma or represent unrelated rocks from the Tertiary Cascade crust beneath the volcano. Heliker (1995) argued that the former might be the case. However, preliminary U-Pb zircon ages of ~25 Ma from three gabbronorite inclusions from the 1980–86 dome complex (Pallister and others, this volume, chap. 30) suggest that these are derived from Tertiary basement incorporated into the Mount St. Helens magmatic system, and trace-element and Pb-isotope analyses of inclusions and plagioclase phenocrysts support this model. Plagioclase crystals analyzed from three gabbronorite inclusions have significantly different trace-element compositions than coexisting plagioclase phenocrysts, with lower Sr and generally higher Ti, Ba, REE, and Pb (fig. 3). There are also small but consistent differences among inclusions, suggesting that some heterogeneity exists in their source (figs. 3, 4). Differences in trace-element abundances between phenocrysts and inclusions suggest that inclusions have equilibrated with a melt of significantly different composition than that from which coexisting phenocryst phases crystallized. Overall, the compositions of plagioclase in gabbroic inclusions

are difficult to relate to those of phenocrysts and to bulk magma composition by any reasonable petrologic model.

The Pb-isotope compositions of plagioclase from inclusions also are consistently different from those of plagioclase phenocrysts and groundmass (fig. 5), with inclusions having lower $^{208}Pb/^{206}Pb$ and $^{207}Pb/^{206}Pb$ than groundmass and phenocrysts. This difference is inconsistent with a simple petrologic relation between inclusions and the host melt, and it specifically argues against inclusions representing a "restite"-like material remaining from melting of metabasalt to produce dacite. Such restite would be expected to have the same Pb-isotope composition as melts unless significant mixing with additional melt or crustal assimilation had occurred.

Lead-isotope composition of groundmass material shows that disaggregation of inclusions also effects the composition of the groundmass on relatively small spatial scales. This phenomenon is particularly evident in SH304-2C, where measurements of the groundmass composition made adjacent to the inclusion lie on an apparent mixing line between the compositions of phenocrysts and plagioclase within gabbroic inclusions (fig. 5). Contributions from disaggregating inclusions also may influence variations in measured $(^{230}Th)/(^{232}Th)$ in plagioclase separates (Cooper and Donnelly, this volume, chap. 36). Such contributions from disaggregation of gabbroic inclusions probably limit the utility of conventional bulk rock or mineral separate-based isotopic measurements for estimating magmatic composition, as these will invariably represent a mixture between the true isotopic composition of the magma and various admixtures of disaggregated and remelted inclusions.

Conclusions

Laser ablation ICP–MS analyses of anorthite content, trace-element (Li, Ti, Sr, Ba, LREE, Pb) concentrations, and Pb-isotope compositions in plagioclase from dacite of the 2004–5 and 1981–86 eruptions of Mount St. Helens provide insight into the petrologic processes leading to formation and eruption of these magmas. Anomalously high Li contents in the early stage of the eruption are thought to reflect addition of Li to the upper part of the magma chamber immediately before eruption (within ~1 year) by transfer of an alkali-enriched exsolved vapor from deep within the mama chamber. Accumulation of Li-rich vapor in the apical part of the magma storage zone may have increased fluid pressures, perhaps helping to initiate eruption. The compositional ranges of other trace elements in plagioclase phenocrysts remain largely constant in material erupted between October 2004 and April 2005 and are broadly similar to those measured in 1981–85 dome samples. These elements show significant correlations with anorthite content that, particularly for Sr and Ti, cannot be described solely by variations in plagioclase–melt partitioning. A simple model involving closed-system fractional crystallization of plagioclase + hypersthene + amphibole + oxides largely reproduces the observed trends, suggesting that plagioclase compositions are predominantly controlled by the degree of crystallinity of the magma and sequestration of compatible elements during crystallization. Analyses from traverses within individual plagioclase phenocrysts generally support this model but also suggest that localized variations exist in the composition of melt from which individual plagioclase crystallize. These analytical differences probably reflect localized variations in phase proportions and crystallinity during magma residence.

Plagioclase from gabbronorite inclusions in three samples has markedly different trace-element and Pb-isotope compositions compared to plagioclase phenocrysts. Inclusions typically have higher Ti, Ba, REE, and Pb and lower Sr and have lower $^{208}Pb/^{206}Pb$ and $^{207}Pb/^{206}Pb$ ratios than coexisting plagioclase phenocrysts. The compositions of plagioclase from gabbroic inclusions appear to be unrelated to phenocryst compositions. We suggest that gabbroic inclusions are samples of the mafic Tertiary basement from beneath the volcano.

Acknowledgments

The facilities of the W.M. Keck Collaboratory for Plasma Mass Spectrometry were used in this work. We would also like to thank the staff of the U.S. Geological Survey David A. Johnston Cascades Volcano Observatory for providing a unique sample set, and the Mount St Helens petrology working group (you know who you are!) for feedback and comments. This work was funded in part by National Science Foundation grant EAR 0440382.

References Cited

Baker, J.A., Peate, D.W., Waight, T., and Meyzen, C., 2004, Pb isotopic analysis of standards and samples using a ^{207}Pb-^{204}Pb double spike and thallium to correct for mass bias with a double-focusing MC–ICP–MS: Chemical Geology, v. 211, p. 275–303.

Berlo, K., Blundy, J., Turner, S., Cashman, K., Hawkesworth, C., and Black, S., 2004, Geochemical precursors to volcanic activity at Mount St. Helens, USA: Science, v. 306, p. 1167–1169.

Bindeman, I.N., Davis, A.M., and Drake, M.J., 1998, Ion microprobe study of plagioclase-basalt partition experiments at natural concentration levels of trace elements: Geochimica et Cosmochimica Acta, v. 62, p. 1175–1193.

Blundy, J.D., and Wood, B.J., 1994, Prediction of crystal–melt partition coefficients from elastic moduli: Nature, v. 372, p. 452–454.

Blundy, J., Cashman, K.V., and Berlo, K., 2008, Evolving magma storage conditions beneath Mount St. Helens inferred from chemical variations in melt inclusions from the 1980–1986 and current (2004–2006) eruptions, chap. 33 *of* Sherrod, D.R., Scott, W.E., and Stauffer, P.H., eds., A volcano rekindled; the renewed eruption of Mount St. Hel-

ens, 2004–2006: U.S. Geological Survey Professional Paper 1750 (this volume).

Browne, B.L., Eichelberger, J.C., Patino, L.C., Vogel, T.A., Uto, K., and Hoshizumi, H., 2006, Magma mingling as indicated by texture and Sr /Ba ratios of plagioclase phenocrysts from Unzen volcano, SW Japan: Journal of Volcanology and Geothermal Research, v. 113, p. 103–116.

Cherniak, D.J., and Watson E.B., 1994, A study of strontium diffusion in plagioclase using Rutherford backscattering spectroscopy: Geochimica et Cosmochimica Acta, v. 58, p. 5179–5190.

Cooper, K.M., and Donnelly, C.T., 2008, ^{238}U-^{230}Th-^{226}Ra disequilibria in dacite and plagioclase from the 2004–2005 eruption of Mount St. Helens, chap. 36 *of* Sherrod, D.R., Scott, W.E., and Stauffer, P.H., eds., A volcano rekindled; the renewed eruption of Mount St. Helens, 2004–2006: U.S. Geological Survey Professional Paper 1750 (this volume).

Couch, S., Sparks, R.S.J., and Carroll, M.R., 2001, Mineral disequilibrium in lavas explained by convective self-mixing in open magma chambers: Nature, v. 411, p. 1037–1039.

Heliker, C., 1995, Inclusions in the Mount St. Helens dacite erupted from 1980 through 1983: Journal of Volcanology and Geothermal Research, v. 66, nos. 1–3, p. 115–135, doi:10.1016/0377-0273(94)00074-Q.

Kelley, K.A., Plank, T., Ludden, J., and Staudigel, H., 2003, The composition of altered oceanic crust at OPD sites 801 and 1149: Geochemistry Geophysics Geosystems, v. 4, no. 6, 21 p., doi:10.1029/2002GC000435.

Kent, A.J.R., and Ungerer, C.A., 2006, Analysis of light lithophile elements (Li, Be, B) by laser ablation ICP–MS; comparison between magnetic sector and quadrupole ICP–MS: American Mineralogist, v. 91, p. 1401–1411.

Kent, A.J.R., Stolper, E.M., Francis, D., Woodhead, J., Frei, R., and Eiler, J., 2004a, Mantle heterogeneity during the formation of the North Atlantic Igneous Province; constraints from trace-element and Sr-Nd-Os-O isotope systematics of Baffin Island picrites: Geochemistry Geophysics Geosystems, v. 5, 26 p., doi:10.1029/2004GC000743.

Kent, A.J.R., Jacobsen, B., Peate, D.W., Waight, T.E., and Baker, J.A., 2004b, Isotope dilution MC–ICP–MS rare earth element analysis of geochemical reference materials NIST SRM 610, NIST SRM 612, NIST SRM 614, BHVO-2G, BHVO-2, BCR-2G, JB-2, WS-1, W-2, AGV-1, AGV-2: Geostandards Newsletter, v. 28, p. 417–430.

Kent, A.J.R., Blundy, J., Cashman, K.V., Cooper, K.M., Donnelly, C., Pallister, J.S., Reagan, M., Rowe, M.C., and Thornber, C.R., 2007, Vapor transfer prior to the October 2004 eruption of Mount St. Helens, Washington: Geology, v. 35, no. 3, p. 231–234, doi:10.1130/G22809A.1.

Pallister, J.S., Thornber, C.R., Cashman, K.V., Clynne, M.A., Lowers, H.A., Mandeville, C.W., Brownfield, I.K., and Meeker, G.P., 2008, Petrology of the 2004–2006 Mount St. Helens lava dome—implications for magmatic plumbing and eruption triggering, chap. 30 *of* Sherrod, D.R., Scott, W.E., and Stauffer, P.H., eds., A volcano rekindled; the renewed eruption of Mount St. Helens, 2004–2006: U.S. Geological Survey Professional Paper 1750 (this volume).

Paul, B., Woodhead, J., and Hergt, J.M., 2005, Improved *in situ* isotope analysis of low-Pb materials using LA–MC–ICP–MS with parallel ion counter and Faraday detection: Journal of Analytical Atomic Spectroscopy, v. 20, p. 1350–1357.

Pearce, N.J.G., Perkins, W.T., Westgate, J.A., Gorton, M.P., Jackson, S.E., Neal, C.R., and Chenery, S.P., 1997, A compilation of new and published major and trace-element data for NIST SRM 610 and NIST SRM 612 glass reference materials: Geostandards Newsletter, v. 21, p. 115–144.

Pearce, T.H., and Kolisnik, A.M., 1990, Observations of plagioclase zoning using interference imaging: Earth Science Reviews, v. 29, p. 9–26.

Rocholl, A., 1998, Major and trace-element composition and homogeneity of microbeam reference material; basalt glass USGS BCR-2G: Geostandards Newsletter, v. 22, p. 33–45.

Rollinson, H., 1993, Using geochemical data; evaluation, presentation, interpretation: Harlow, U.K., Longman Scientific and Technical, 352 p.

Rowe, M.C., Thornber, C.R., and Kent, A.J.R., 2008, Identification and evolution of the juvenile component in 2004–2005 Mount St. Helens ash, chap. 29 *of* Sherrod, D.R., Scott, W.E., and Stauffer, P.H., eds., A volcano rekindled; the renewed eruption of Mount St. Helens, 2004–2006: U.S. Geological Survey Professional Paper 1750 (this volume).

Rutherford, M.J., and Devine, J.D., III, 2008, Magmatic conditions and processes in the storage zone of the 2004–2006 Mount St. Helens dacite, chap. 31 *of* Sherrod, D.R., Scott, W.E., and Stauffer, P.H., eds., A volcano rekindled; the renewed eruption of Mount St. Helens, 2004–2006: U.S. Geological Survey Professional Paper 1750 (this volume).

Streck, M.J., Broderick, C.A., Thornber, C.R., Clynne, M.A., and Pallister, J.S., 2008, Plagioclase populations and zoning in dacite of the 2004–2005 Mount St. Helens eruption; constraints for magma origin and dynamics, chap. 34 *of* Sherrod, D.R., Scott, W.E., and Stauffer, P.H., eds., A volcano rekindled; the renewed eruption of Mount St. Helens, 2004–2006: U.S. Geological Survey Professional Paper 1750 (this volume).

Triebold, S., Kronz, A., and Wörner, G., 2005, Anorthite-calibrated backscattered electron profiles, trace elements and growth textures in feldspars from the Teide-Pico Viejo volcanic complex (Tenerife): Journal of Volcanology and Geothermal Research, v. 154, p. 117–130.

Zellmer, G.F., Sparks, R.S.J., Hawkesworth, C.J., and Wiedenbeck, M., 2003, Magma emplacement and remobilization timescales beneath Montserrat; insights from Sr and Ba zonations in plagioclase phenocrysts: Journal of Petrology, v. 44, p. 1413–1431.

Appendix 1. Supplementary Analytical Data for Glass Standard BCR-2G and for Pb-Isotope Compositions of Plagioclase and Groundmass in 2004–2005 Mount St. Helens Dome Samples

Data for seven replicate analyses of glass standard BCR-2G were determined during this study, and a comparison with accepted concentrations is listed in table 4. Table 5 lists $^{208}Pb/^{206}Pb$ and $^{207}Pb/^{206}Pb$ ratios of plagioclase phenocrysts, groundmass, and plagioclase within gabbroic inclusions from three samples of the Mount St. Helens dome erupted in 2004–2005 measured by laser-ablation multicollector ICP–MS. The average of four replicate isotopic analyses from glass standard BCR-2G is included in table 5 for reference.

Table 4. Analytical data from replicate analysis of USGS glass standard BCR-2G.

[Average of seven analyses. CaO/SiO_2 ratios calculated from equation 1 (see text). "Accepted values" compiled from these sources: rare-earth elements from Kent and others (2004b); Li from Kent and Ungerer (2006); Si from Rocholl (1998); all other elements from Kelley and others (2003).]

BCR-2G ----------	Accepted (µg/g)	Measured (µg/g)	± 2σ
Li	10.5	11.2	3.0
Ti	13,500	12,047	490
Sr	346	339	13
Ba	674	624	25
La	25.3	23.1	0.9
Ce	53.7	50.8	2.5
Pr	6.9	6.3	0.5
Nd	28.8	26.2	1.8
Eu	1.9	1.8	0.2
Pb	11.0	11.8	0.7
CaO/SiO_2	0.13	0.12	0.02

Table 5. Pb-isotope compositions of plagioclase and groundmass in 2004–2005 Mount St. Helens dome samples.

[Analysis by laser-ablation multicollector ICP–MS at Oregon State University. Values are isotopic ratios and, parenthetically, their 1σ uncertainties expressed in the final decimal places. "Inclusions" refers to plagioclase in gabbroic inclusions. Average of four replicate isotopic analyses from glass standard BCR-2G included for reference.]

	$^{208}Pb/^{206}Pb$		$^{207}Pb/^{206}Pb$	
SH304-2A				
Phenocryst	2.0495	(62)	0.8309	(29)
Phenocryst	2.0507	(48)	0.8311	(22)
Phenocryst	2.0443	(35)	0.8275	(16)
Phenocryst	2.0443	(27)	0.8260	(18)
Phenocryst	2.0466	(22)	0.8255	(14)
Groundmass	2.0478	(11)	0.8283	(6)
Groundmass	2.0489	(9)	0.8285	(5)
Groundmass	2.0474	(11)	0.8276	(5)
Groundmass	2.0466	(5)	0.8277	(5)
Groundmass	2.0477	(8)	0.8271	(7)
SH304-2C				
Phenocryst	2.0459	(10)	0.8277	(4)
Phenocryst	2.0505	(38)	0.8310	(12)
Groundmass	2.0451	(15)	0.8275	(9)
Groundmass	2.0465	(11)	0.8278	(8)
Groundmass	2.0451	(9)	0.8275	(1)
Groundmass	2.0465	(8)	0.8278	(1)
Groundmass	2.0429	(12)	0.8234	(1)
Groundmass	2.0420	(4)	0.8245	(1)
Groundmass	2.0398	(12)	0.8234	(1)
Inclusion	2.0407	(9)	0.8209	(4)
Inclusion	2.0397	(11)	0.8206	(4)
Inclusion	2.0403	(17)	0.8216	(7)
Inclusion	2.0397	(14)	0.8209	(6)
SH306-1				
Phenocryst	2.0478	(33)	0.8288	(19)
Phenocryst	2.0457	(49)	0.8293	(33)
Groundmass	2.0468	(7)	0.8269	(6)
Groundmass	2.0470	(14)	0.8272	(5)
Groundmass	2.0472	(15)	0.8287	(9)
Inclusion	2.0420	(7)	0.8204	(3)
Inclusion	2.0369	(15)	0.8193	(5)
Inclusion	2.0362	(9)	0.8192	(6)
Inclusion	2.0396	(12)	0.8198	(7)
Inclusion	2.0378	(23)	0.8213	(11)
Inclusion	2.0369	(17)	0.8208	(9)
Inclusion	2.0397	(17)	0.8234	(9)
BCR-2G (n=4)	2.0637	(10)	0.8316	(5)

Appendix 2. Anorthite Content and Trace-Element Abundances in Five Plagioclase Grains from Dome Sample SH304-2A

[This appendix appears only in the digital versions of this work—in the DVD-ROM that accompanies the printed volume and as a separate file accompanying this chapter on the Web: at http://pubs.usgs.gov/pp/1750.]

Appendix 2 is a spreadsheet that lists the mole fraction anorthite and measured concentrations for six elements (Li, Ti, Sr, Ba, La, Ce) from one traverse across each of five plagioclase grains. Traverses range in length from 375 to 775 μm.

Appendix 3. Anorthite and Trace Element Abundances in Plagioclase from 2004–2005 and 1981–1985 Dome Samples from Mount St. Helens

[This appendix appears only in the digital versions of this work—in the DVD-ROM that accompanies the printed volume and as a separate file accompanying this chapter on the Web at http://pubs.usgs.gov/pp/1750.]

Appendix 3 is a spreadsheet that lists the mole fraction anorthite and analytical data for 10 elements (Li, Ti, Sr, Ba, La, Ce, Pr, Nd, Eu, Pb) from 203 analyses of plagioclase phenocryst cores, margins, and inclusions in eight sample erupted in 2004–2005. Also shown are 28 analyses of plagioclase phenocryst cores in three samples erupted during the period 1981–85.